FORMING LIMITS OF TUFF COMPOSITES IN STRETCH FORMING PROCESSES

Thomas A. Cender[1], Henry Fidlow[1,2], Shridhar Yarlagadda[1], Dirk Heider[1], Pavel Simacek[1,2], Suresh G. Advani[1,2], John W. Gillespie Jr.[1,2]

[1] Center for Composite Materials, University of Delaware, Newark, DE 19716
[2] Department of Mechanical Engineering, University of Delaware, Newark, DE 19716

ABSTRACT

Tailored universal Feedstock for Forming (*TuFF*) is an aligned discontinuous fiber composite material which is able to achieve 60% fiber volume fraction and aerospace equivalent properties due to its high degree of fiber alignment. One advantage of the discontinuous fiber format is that TuFF composites can stretch form biaxially to produce complex geometry parts, which cannot otherwise be produced with continuous fiber reinforcement. Ply extensibility in the fiber direction is governed by the relative longitudinal displacement of neighboring short fibers. An important feature in understanding the formability of an aligned discontinuous fiber composite, is the effect of strain on the composite microstructure and the resulting structural performance. In this work, the microstructure of thermoplastic *TuFF* composites is analyzed with X-ray micro-CT to determine the evolving microstructural changes with increasing magnitude of strain. In-situ Digital Image Correlation, is used to visualize localizing defects which lead to the onset of material tearing. DIC can be used to determine abrupt material failures which occur at high strain rates. At low strain rates the microstructure evolution with applied strain is more gradual and statistical in nature and microscopy (optical or X-ray micro-CT) is more suitable to quantify these changes.
Keywords: Composite Forming, Thermoplastic, Discontinuous Carbon Fiber, TuFF
Corresponding author: Thomas A. Cender
DOI: (Will be added by SAMPE)

1. INTRODUCTION

Tailored Universal Feedstock for Forming (*TuFF*) is process developed by the Center for Composite Materials at the University of Delaware [1] for producing highly aligned discontinuous fiber composite materials [2]. An exceptionally high degree of fiber alignment [3] allows fiber volume fraction up to 60% and structural performance equivalent to aerospace grade continuous fiber composites [1,4]. *TuFF* aligned short fibers can currently be prepregged with any resin system to any fiber areal weight greater than or equal to 60 grams per square meter (gsm). Unidirectional prepreg plies are stacked to build a flat blank laminate structure. The discontinuous fiber format enables lamina extension in the fiber direction, which allows forming of complex featured structures which require biaxial stretching of a blank [5].

Figure 1 schematically shows features of an aligned fiber microstructure. Alignment distribution, fiber end gap size and staggering have a large influence on both the mechanical performance and the formability. In forming processes, blanks are preheated to bring the matrix material (either thermoset or thermoplastic) to a viscous state. This allows the matrix to flow and translate the short

DOI: (Will be added by SAMPE)

fibers, which are inextensible. As the blank undergoes deformation during forming, the microstructure must accommodate the rearrangement. Adjacent fibers will shear relative to one another. In the simplest framework, this process draws fibers closer together (transverse contraction at constant volume) and extends fiber end gaps. The degree to which fibers can reduce their spacing is very limited at high fiber volume fractions. When a physical limit is reached, the polymer matrix will cavitate and progress into tearing. Porosity during the stretching process is not an issue in and of itself, so long as the laminate can be consolidated to a uniform material without persisting porosity after forming.

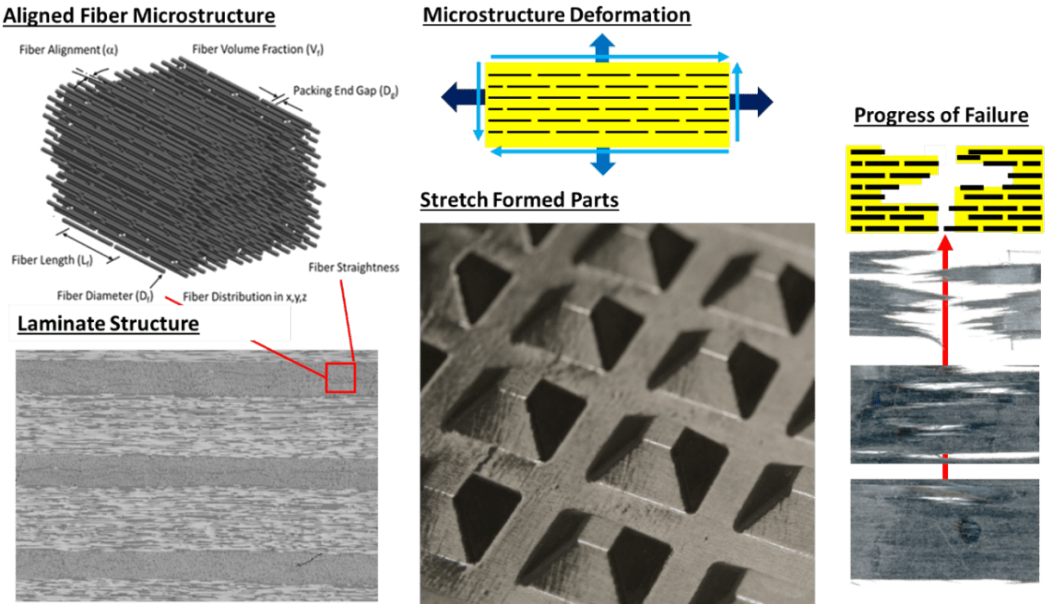

Figure 1. Aligned TuFF Fibers are prepregged and laminated to produce a flat blank [2]. Blanks are biaxially stretch formed to produce complex part geometry [3]. Material deformation during forming rearranges the ply microstructure. A forming limit will be defined by the influence of strain and strain rate on the material quality in the formed part

The goal of this work is to determine the mechanisms contributing to the forming limit of a thermoplastic matrix *TuFF* blank subject to longitudinal (fiber direction) extension. A definition of failure must be formulated which is appropriate for stretch formed *TuFF* composites. Failure can either be abrupt or gradual and will depend on both the level of strain and the strain rate. During forming material relaxation (temperature dependent) competes with the imposed strain rate (cycle times) so forming limits are expected to be both temperature and rate dependent. High strain rates induce high stress levels and can be expected to initiate tearing at lower levels of strain. At infinitely low strain rates, microstructure can rearrange with sufficient time for polymer to flow and stress to relax. From an experimental perspective, the effect of strain level on microstructure can be more easily studied at low strain rate and isothermal conditions.

Thermoplastic composites are typically formed at high strain rates. Hot blanks are shuttled into a cold press. Press closing speed is chosen such that the material will form before cooling to a glassy or crystalline state. The deformation of the blank is completed in 2-10 seconds, which corresponds approximately to strain rates of 10^{-2} to $5 \times 10^{-2}\ s^{-1}$ for a forming strain of 10%. In studying the mechanisms of failure, it is important to delineate failures due to high strain rate vs. high strain.

DOI: (Will be added by SAMPE)

Two characterization approaches are employed. Longitudinal strain during forming is evaluated at the continuum scale by analyzing stress-strain data, dimensional changes, and with Digital Image Correlation (DIC) of surface strain. Then the material microstructure is evaluated from optical micrographs of material cross-sections and 3D X-ray micro-CT. It is found that abrupt tearing at high strain rates is easily observed on the continuum scale; however, no clear transition to localization was observable at high levels of strain when the strain rate is low. For this, microscopy and CT were able to capture the trend of material variability at high levels of longitudinal strain.

2. MATERIALS AND METHODS

For these studies, unidirectional *TuFF* composites were prepared from 3mm long IM7 fibers and Ultem 1000 thermoplastic PEI. Each ply consisted of 120gsm fiber areal weight. PEI resin content was set to produce a composite ply of 57% fiber volume fraction. Laminates were produced by resin film infusion in an autoclave at 20.6bar (300psi) and 330°C. Material prepared for DIC analysis consisted of a single ply, $[0]_1$, while material prepared for microstructure analysis consisted of 6 plies, $[0]_6$. Average thickness of the consolidated material was 123±3µm and 725±8µm respectively. Figure 2 shows cross-sections of the $[0]_6$ sample across the 0-degree and 90-degree fiber directions. Previous work has measured the fiber alignment to be 95% within ±5-degrees [2]. From the 0-degree cross-section, a small number of grossly misaligned fibers—referred to as *rogue fibers*—are evident as elliptical cross-sections and resin rich lines. The current level of rogue fibers is deemed acceptable since mechanical performance was demonstrated to be equivalent to continuous fiber composite [1].

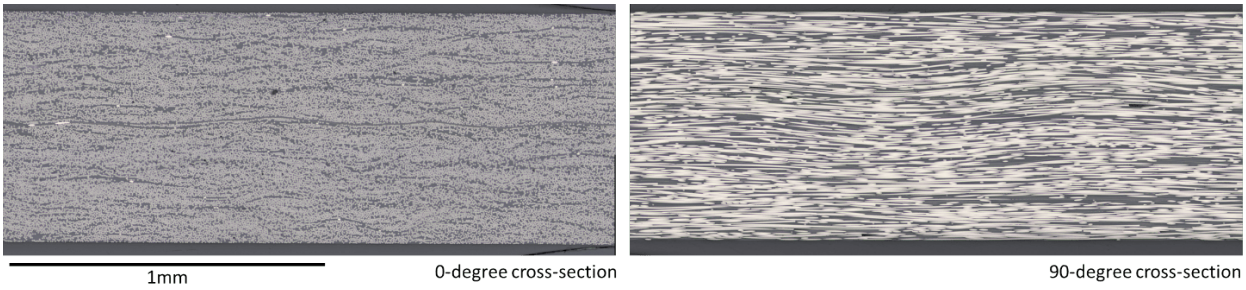

Figure 2. Tuff/PEI $[0]_6$ consisting of 3mm IM7 fibers. Fiber areal weight is 120gsm/ply.

To study the effect of strain and strain rate on the material microstructure, all samples were stretched longitudinally along the fiber direction using an Instron 4484 Universal Testing Machine (UTM). An environmental chamber was used to elevate the temperature of the samples up to 330°C—the target forming temperature for PEI composites. The crosshead speed was set to increase logarithmically to impose a constant true strain rate in the samples. A 500N load cell was chosen based on the load range of 20-200N observed during testing. The Instron was equipped with a single camera video extensometer to measure strain on the sample surface.

Samples were cut with a slot grinder from 254mm x 254mm (10in x 10in) panels to obtain 25.4mm (1in) wide specimens. The $[0]_1$ samples were reduced to a length of 177mm (7in) and a speckle pattern was applied with white high temperature spray paint to a 3” length between grips. The $[0]_6$ samples were kept 254mm (10in) long to obtain a 152mm (6in) length between grips. Two white

DOI: (Will be added by SAMPE)

dots were painted on the $[0]_6$ samples at vertical spacing of 25.4mm (1in) in order to use the marker tracking feature of the video extensometer to measure strain in the central portion of the specimens. Metal end tables were sand blasted and clamped to the specimens during fixturing; failure at the grips was not observed.

To understand the effect of temperature and strain rate on formability, $[0]_1$ samples were stretched to ~10.5% elongation, to halt the material at a true strain of $\varepsilon_1 = 0.1$. Strain rates of $\dot{\varepsilon}_1 = 10^{-4}, 10^{-3}, 10^{-2}, 5 \times 10^{-1}, 10^{-1}\ s^{-1}$ were tested isothermally at temperatures $T = 280, 300, 310, 320, 330$ ℃. To characterize the effect of strain on the sample microstructure, $[0]_6$ samples were stretched at of $\dot{\varepsilon}_1 = 10^{-3} s^{-1}$, $T = 330$ ℃ to 4, 10, 20, 33, 50, and 68% elongation which corresponds to a true strain of $\varepsilon_1 = 0.039, 0.098, 0.18, 0.29, 0.40, 0.52$ respectively. Figure 3 show examples of specimens of TuFF/PEI $[0]_1$ (a) and $[0]_6$ (b) after testing.

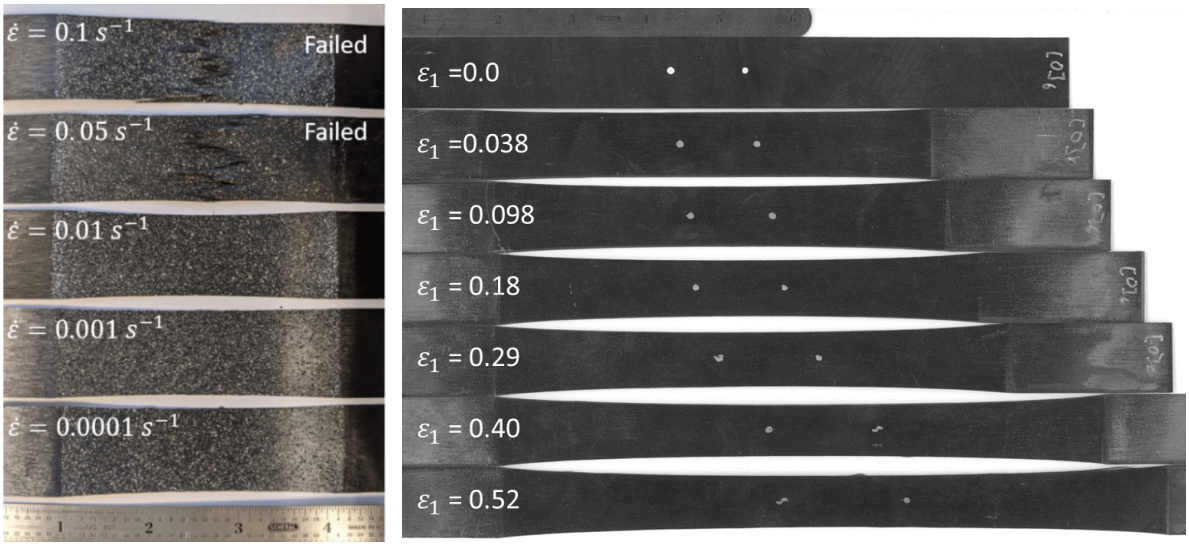

(a) (b)

Figure 3. (a) TuFF/PEI $[0]_1$ tested at $T = 330$ ℃ at varying strain rates. Each test was halted at $\varepsilon_1 = 0.1$. (b) TuFF/PEI $[0]_6$ tested at $T = 330$ ℃ with a strain rate of $\dot{\varepsilon}_1 = 10^{-3} s^{-1}$. Tests were halted at increments of true strain (ε_1) up to 0.52 for microstructure evaluation.

Finally, a thermomechanical analyzer (TMA) was used to measure the deconsolidation of free-standing *TuFF*/PEI $[0]_6$ specimens during heating to the target forming temperature of 330°C. This provides an understanding of the initial microstructure prior to stretching. All samples were dried for 16 hours at 120°C prior to testing.

3. RESULTS AND DISCUSSION

3.1 Continuum Scale Characterization

Mechanical testing is often a good first evaluation of material structure. Rheology can offer insight into molecular order and uniaxial tensile response can be related to damage in materials. While stretching *TuFF* specimens in the UTM, the simplest indication of failure is expected to arise from features in the stress strain response. For convention, material directions 1, 2, and 3 refer to the longitudinal fiber direction, transverse direction in the plane of the laminate, and transverse through thickness direction respectively. All stress strain data is reported in terms of true stress

DOI: (Will be added by SAMPE)

($\sigma_1 = F(1+\epsilon)/A_0$) and true strain ($\varepsilon_1 = \ln(1+\epsilon)$). This is essential for relating material response to volume changes. Large deformations in materials are known to be a constant volume process. This is written mathematically as the product of the stretches $\lambda_1\lambda_2\lambda_3 = lwt/(lwt)_0 = 1$ or $\varepsilon_1 + \varepsilon_2 + \varepsilon_3 = 0$. As stated above, the material porosity is expected to increase during stretching so the constant volume assumption can be extended only to the resin and fiber phases, excluding porosity. This expression can be rewritten to include porosity (ϕ)

$$\frac{lwt(1-\phi)}{[lwt(1-\phi)]_0} = 1 \qquad \text{Eq. 1}$$

where length (l), width (w), and thickness (t) are measured externally on the sample before and after deformation. If initial porosity is zero ($\phi_0 = 0$) then Eq. 1 can relate material porosity to local strain

$$\varepsilon_1 + \varepsilon_2 + \varepsilon_3 = -\ln(1-\phi)$$

The use of true strain assumes that the current 'material' cross-sectional area (A) reduces under a constant volume process where $A = A_0/(1+\epsilon)$. Here $\epsilon = l/l_0 - 1$ is the longitudinal engineering strain and $A_0 = w_0 t_0(1-\phi_0)$ is the initial 'material' cross-sectional area at the onset of the test. Since volume is only conserved in the 'material' (resin and fibers), A and A_0 reference the non-porous cross-sectional area. Initial and final width and thickness (w_0, t_0, w, and t) are measured as the external sample dimension. Porosity (ϕ)—as it evolves through the process—is an unknown and will be measured and validated using microscopy. Therefore, this expression for current cross-sectional area A is an assumption which will be verified in the microstructure evaluation. As shown in Figure 2, the initial consolidated material has no porosity, so $A_0 = w_0 t_0$ is measured from the consolidated material state in order to define a known 'material' cross-sectional area.

Figure 4a shows the stress strain response of the $[0]_6$ specimen stretched to $\varepsilon_1 = 0.52$ (68% elongation at $T = 330$ ℃ with a strain rate of $\dot{\varepsilon}_1 = 10^{-3}s^{-1}$. The response of this material is viscous only and is discussed in a separate work [6]. A purely viscous material loaded at constant strain rate should maintain a constant level of stress; therefore, the stress decay observed in Figure 4a is due to microstructural features. This phenomenon has been observed [7] and modeled [8] for longitudinal extension aligned discontinuous fiber composites. Simacek and Advani (2018) [8] show that this behavior arises from the change in fiber end gap length. This study also proposes that this trend may arise due to increased porosity. In either case, Figure 4a presents no discernable indication of failure which may be used to determine degradation of the structural performance. The series of samples in Figure 3b are further evaluated with microscopy.

Figure 4b shows the effect of strain rate on the stress strain response for $[0]_1$ specimens. Here, the tests were halted at $\varepsilon_1 = 0.1$. The large change in stress is due to polymer shear thinning [6]. At strain rates below $10^{-2}s^{-1}$, the stress remains relatively constant on the log scale. Specimens strained at 5×10^{-2} and $10^{-1}s^{-1}$ show a more abrupt drop in stress on the log scale. Failure in these specimens is clearly seen with DIC to initiate at $\varepsilon_1 = 0.04$.

The methodology for the results in Figure 4b were repeated at lower temperatures. Figure 5 shows the maximum stress for each strain rate and temperature tested. Circle markers indicate samples which did not show any signs of tearing before $\varepsilon_1 = 0.1$ was reached. The DIC strain map for these samples show period variability on the length scale of 3-5mm. This can be taken as some

DOI: (Will be added by SAMPE)

measure of uniformity or non-uniformity in the extensional behavior of the *TuFF* micro-structure. In terms of formability and defining failure, some non-uniformity is acceptable as long as it is below a certain threshold. Here, the pattern is consistent over the entire gage length, and a localized band of necking or tearing is not present. This method does not offer enough information in to define a material forming limits. Future work will measure mechanical properties after forming and consolidation to establish forming limits for structural components.

In Figure 5, samples in which tearing can be seen visually (as in Figure 3a) are marked with 'x'. This is supported by surface strain data from DIC, where high strain is localized in a small band spanning the width of the sample. The results at lower temperatures suggest that early on-set of failure (below 10% elongation) is related to stress more than strain rate. All samples which exceeded 25MPa failed below 10% elongation.

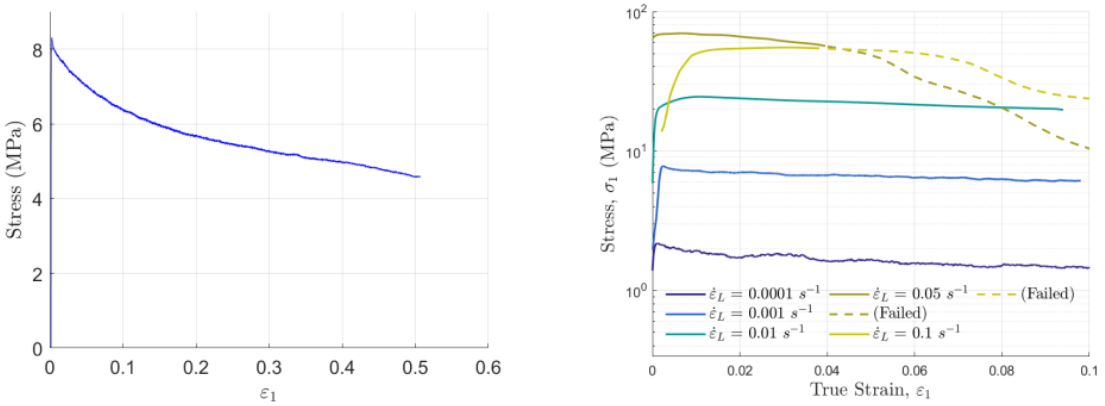

Figure 4. (a) Linear scale of the (true) stress (true) strain response of TuFF/PEI $[0]_6$ at $T = 330$ ℃ at $\dot{\varepsilon}_1 = 10^{-3}s^{-1}$. The test was halted at $\varepsilon_1 = 0.52$ and prepared for microscopy. (b) Log scale of the (true) stress (true) strain response of TuFF/PEI $[0]_1$ at $T = 330$ ℃ for a range of strain rates. Each test was halted at $\varepsilon_1 = 0.1$.

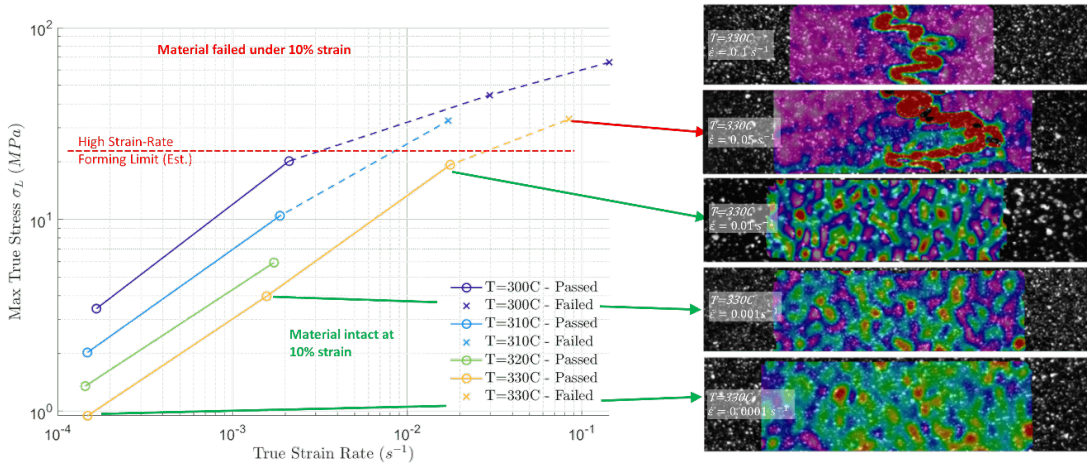

Figure 5. TuFF/PEI $[0]_1$ tested at a range of strain rates and temperatures. Each test was halted at $\varepsilon_1 = 0.1$. The maximum true stress is reported from each stress strain curve. Tearing can be observed in DIC data for all samples which exceeded 25MPa.

DOI: (Will be added by SAMPE)

3.2 Microscale Characterization

A thermomechanical analyzer (TMA) was used to measure the deconsolidation of *TuFF*/PEI $[0]_6$ specimens during heating to the target forming temperature of 330°C. Deconsolidation of thermoplastic composite blanks is the result of heating a consolidated blank. Left unconstrained, the material returns to an uncompressed state, primarily driven by the relaxation of fiber stress [9]. Prior to forming, blanks are heated to melt the polymer. Hot blanks are shuttled into a mold and pressed in order to form and reconsolidate the material. The deconsolidated material state is an initial condition of the material as it undergoes deformation during forming. Samples of TuFF/PEI $[0]_6$ with an initial thickness of 728µm were cut to 10mm x 10mm. A 10mm diameter quartz disk was placed over the samples to distribute the area of the probe. Sample were heated at 5°C /min to 330°C and held for 2 hours before cooling back to room temperature. The test was repeated at 0.01N and 0.1N of probe force, applying 0.14 and 1.4kPa (0.02 and 0.2psi) of pressure respectively. Once above the glass transition temperature (217°C), thickness increases rapidly as the polymer matrix soften to allow fiber stress to relax. Thickness growth was not attributed to moisture since samples were appropriately dried and did not measure any mass loss after the cycle.

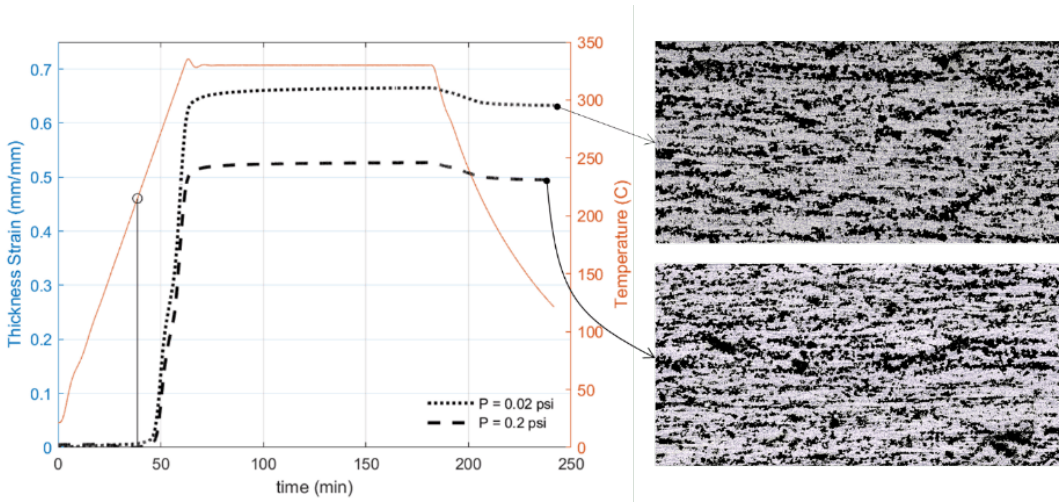

Figure 6. TMA results show that *TuFF*/PEI $[0]_6$ will deconsolidate to 50% thickness growth and generate 33% porosity in the ply. The results are sensitive to the probe force applied. Image segmentation was used to color porosity black in the micrographs.

Samples saw a deconsolidation thickness growth of 63% at 0.14kPa (0.02psi) and 50% at 1.4kPa (0.2psi). This level of growth is higher than a typical continuous fiber composite blank. This is not entirely surprising since the fiber alignment of typical continuous fiber unidirectional tape is slightly higher than *TuFF*. Additionally, the rogue fibers will have a larger contribution to deconsolidation since this process related to fiber alignment and relaxation of elastic bending stress from fibers.

Figure 6 shows micrograph cross-sections of each sample after the thermal cycle. Interestingly, the pattern of porosity is well distributed across the sample cross-section. Studies by Slange et al. [9] demonstrate that the level of deconsolidation is tightly linked to formability. What can also be

DOI: (Will be added by SAMPE)

surmised from the micrographs by Slange et al. is that higher non-uniformity likely has a strong effect. Although the deconsolidation driven thickness growth of TuFF is large, the relative pore size is small. Large splitting or delamination is not observed in these samples.

Using Eq. 1 a porosity of 38% and 33% for the 0.14 and 1.4kPa (0.02psi and 0.2psi) respectively is estimated from the thickness strain. The micrograph images were segmented to measure a porosity of 34.4% and 31.8% respectively—indicating that a probe pressure of 1.4kPa (0.2psi) with 50% thickness growth is more characteristic of ply level deconsolidation.

To understand the change to micro-structure to due longitudinal stretching, samples of *TuFF*/PEI $[0]_6$ (shown in Figure 2b) strained to $\varepsilon_1 = 0.039, 0.098, 0.18, 0.29, 0.40, 0.52$ were sectioned to evaluate the microstructure. The two primary microstructure characteristics being investigated are porosity and thickness. To determine the level and variability of these quantities as a function of longitudinal strain, full sample cross-sections were evaluated with optical microscopy and 3D x-ray micro-CT.

A Bruker Skyscan 1172 micro-CT was used to scan 25mm length of full width sample gage sections. To view the entire sample width, a resolution of 5.95µm/pixel was used for each scan. Reconstructed material cross-sections were segmented (with a Matlab script) to remove porosity. Cross-sectional area and thickness were measured for each slice. Slices were reassembled to produce a flattened image of the gage area with measured thickness (excluding porosity) at each pixel. Figure 7 (left) shows the reassembled flattened images overlaid on the gage section of each specimen. Thickness measured from the flattened images is shown in the contour plot adjacent to the specimen they were collected from. On the right is a representative reconstructed cross-section.

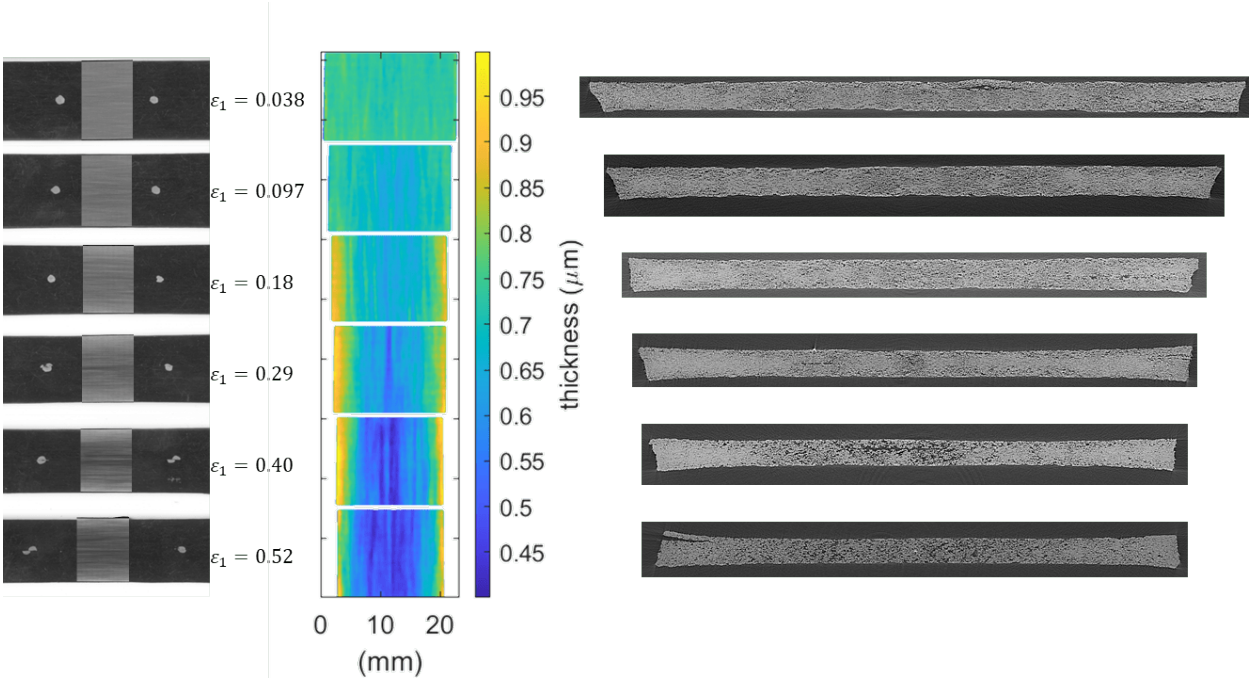

Figure 7. *TuFF*/PEI $[0]_6$ prepared at increasing levels of strain were analyzed with X-ray micro-CT. The full width in the gage section of each sample was scanned at a resolution of 5.95µm/pixel.

DOI: (Will be added by SAMPE)

The contour plot shows thickness measured from reconstructed cross-sections with porosity removed (i.e. the hypothetical consolidated thickness).

The thickness represented in contour plot has porosity excluded in order to understand the amount of 'material' at each point. During the reconsolidation phase, porosity must be suppressed with high transverse pressure. The contour plot evaluates the hypothetical consolidated ply thickness. Thickness is averaged over a moving window 125µm x 125µm, chosen based on a single ply thickness. Thinning of the samples can be clearly observed as the level of strain increases. The uniformity of this thinning will be compared to optical micrographs. Another important point to note from this plot, which can also be seen in the reconstructed cross-sections, is that the edges of the specimen increase in thickness.

Figure 8 shows a DIC strain map of a full sample area between the grips (*TuFF*/PEI $[0]_1$ tested at $T = 330$ ℃ and $\dot{\varepsilon}_1 = 10^{-3}s^{-1}$). The transverse strain is expected to be negative as the specimen width contracts during extension (see Figure 3). The unusual observation here is that there is a large variation in transverse strain from the center line to the edges.

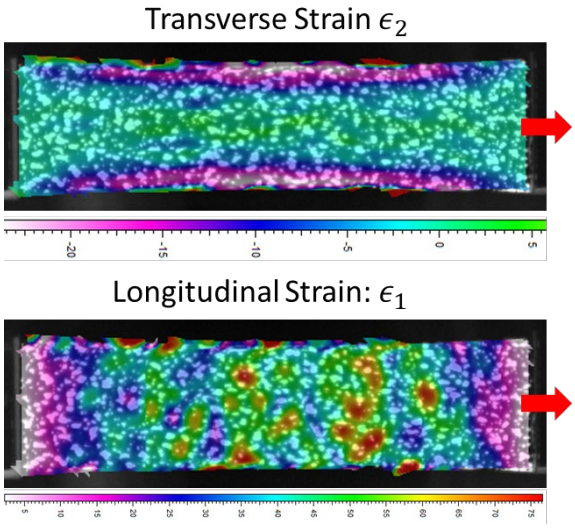

Figure 8. TuFF/PEI $[0]_6$ tested at $T = 330$ ℃ and $\dot{\varepsilon}_1 = 10^{-3}s^{-1}$. Transverse strain is shown to vary across the width of the gage length.

When comparing the material cross-sections in Figure 7 to the transverse strain measured in Figure 8, it's clear that when edges of the samples experience more transverse compressive strain, material accumulates in these regions, while along the centerline the low transverse strain causes the material to thin faster in this strain mode. The material along the centerline of the sample by comparison has higher porosity. This non-uniformity across the sample width, as discussed, is likely due to high anisotropy, which in terms of viscosity is 10^5 times higher in the fiber direction. This testing artifact clearly shows that a true uniaxial tensile strain mode was not achieved.

Optical micrographs were obtained for the full width cross-section of the gage length. Samples were potted in resin with a black dye in increase contrast between the prepreg resin and potting resin in order to distinguish porosity. One cross-section was analyzed for each sample. Images were stitched from 10x magnification from a Keyence VK laser confocal microscope. Figure 9

DOI: (Will be added by SAMPE)

shows micrographs of the central portion of each sample. For comparison the first micrograph in the stack was taken from the material deconsolidated in the TMA, where porosity increased without axial or transverse strain. The micrographs were segmented to measure porosity (which was colored black after analysis). Porosity was measure for each column of pixels through the thicknesses in order to observe the variability in porosity. Local through-thickness porosity is averaged with a moving window of 125µm, corresponding to a single ply thickness. A plot of porosity vs width location is overlayed in red on each micrograph. The vertical scale of each line is between 0 and 1. The average and standard deviation of porosity across the width is plotted relative to the longitudinal strain of the sample they were collected from.

At low axial strain, the porosity relative the initial state observed after deconsolidation is substantially reduced. The force required to strain the material axially is much larger than for transverse strain (3-direction). This causes the material to collapse, without significant resistance, to a more consolidated state. This observation indicated that the deconsolidated material cross-section from Figure 7 evolves as it deforms. As axial strain increases for successive samples, average porosity and porosity variability also increase. In terms of material forming limits, a clear cut off still cannot be deduced. The average porosity increase is less of a concern than the observed increase in variability. Porosity can be consolidated as long as it is uniform on length scale related to the ply thickness. As the material becomes more non-uniform, either the consolidated ply thickness will become more non-uniform or the transverse pressure will not fully consolidate the material, leaving unremoved porosity.

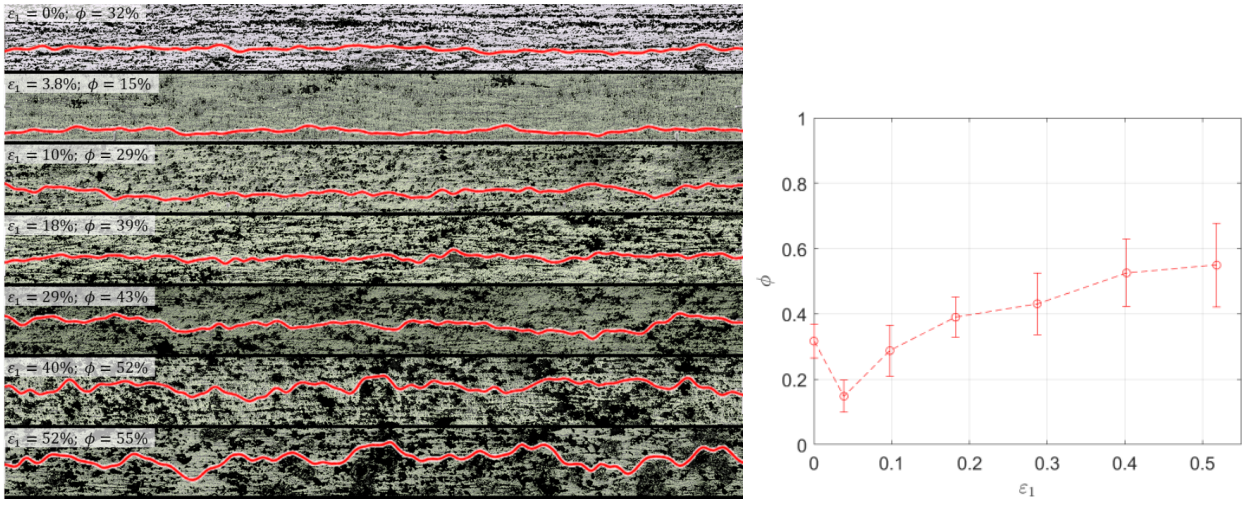

Figure 9. *TuFF*/PEI $[0]_6$ prepared at increasing levels of strain at 330°C were cross-sectioned and visualized with an optical microscope. The images were segmented to measure porosity. Porosity was integrated through the thickness and shown to vary across the width. The average and standard deviation of through-thickness porosity is shown in the graph relative to the applied longitudinal strain.

As discussed in section 3.1, true stress is reported as the applied force over the current 'material' cross-sectional area. The current cross-sectional area is calculated with the assumption that 'material' (fibers and resin only) deformation is a constant volume process, i.e. the 'material' is incompressible. Porosity is excluded from the 'material' cross-section because it cannot transfer load. Without microscopy, the level or porosity is unknown. The non-porous 'material' cross-

DOI: (Will be added by SAMPE)

sectional area was measured from the optical micrographs and X-ray micro-CT volume reconstructions. Figure 10 shows the 'material' cross-sectional area measured with each method. show that the measured total material cross-sectional area closely follows the assumption, and that true stress adequately represents the instantaneous material state.

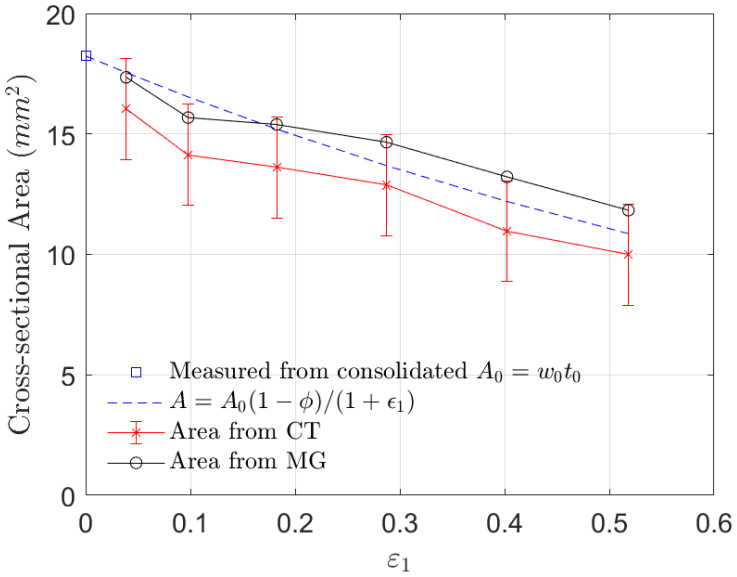

Figure 10. The cross-sectional area reduction calculated from the constant volume assumption is supported by measurements of full width sample in the gage length obtained by both X-ray micro-CT and optical micrographs (MG).

4. CONCLUSIONS

The forming limits of aligned discontinuous fiber *TuFF* composites in longitudinal (fiber direction) extension are evaluated with respect to forming rate and forming strain. In longitudinal extension, aligned fibers shear relative to one another, allowing the macroscopic material to elongate. As ply scale deformation takes place, the microstructure must transfer load between fibers, as well as accommodate the rearrangement of fibers to reflect the required change deformation of the volume.

Two types of mechanisms are discussed in defining failure for formability. At high strain rates, abrupt tearing will occur at low levels of strain. It is proposed that this is due to insufficient time for the material to relax. For TuFF/PEI with 57% fiber volume fraction, failure was observed at all forming range temperatures when stress exceeded 25MPa. In the limit of low strain rate, the micro-structure has sufficient time to relax, and the challenge is for the material to accommodate the deformation. At 57% fiber volume fraction, fibers do not have sufficient space to increase their packing fraction, and thus at high levels of strain, the primary mechanism for deformation is cavitation. This leads to a gradual increase in porosity with longitudinal strain. The porosity is not viewed as a problem in that porosity can be consolidated during forming. However, the gradual increase in material variability will eventually lead to irregular ply thickness and unconsolidated porosity.

DOI: (Will be added by SAMPE)

From these results, guidelines for process setpoints and part geometry can start to be established to meet required material quality and production rate requirement. Failure due to high forming rates will likely present as abrupt tearing, whereas failure due to over stretching will appear as overly thin and irregular ply thicknesses with porosity. Strict forming limits will have to be established relative to the process being used and the strength of the material produced.

5. REFERENCES

1. Yarlagadda, S., Deitzel, J., Heider, D., Tierney, J., & Gillespie, J. W. (2019). Tailorable Universal Feedstock for Forming (TuFF): Overview and Performance. In: SAMPE 2019 - Charlotte, NC. Proceedings
2. Such, M., Ward, C., & Potter, K. (2014). Aligned Discontinuous Fibre Composites: A Short History. *Journal of Multifunctional Composites*, *2*(3), 155–168. https://doi.org/10.12783/issn.2168-4286/2/3/4
3. Heider, D., Tierney, J., Henchir, M. A., Gargitter, V., Yarlagadda, S., Gillespie, J. W., Sun, J., Sietins, J. M., & Knorr, D. (2019). Microstructural Evaluation of Aligned, Short Fiber TuFF Material. In: SAMPE 2019 - Charlotte, NC. Proceedings
4. Heider, D., Tierney, J., Deitzel, J., Kubota, M., Thiravong, J., Gargitter, V., Burris, W., Morris, J., Shevchenko, N., Yarlagadda, S., & Gillespie, J. W. (2019). Closed Loop Recycling of CFRP into Highly Aligned High Performance Short Fiber Composites Using the TuFF Process. In: SAMPE 2019 - Charlotte, NC. Proceedings
5. Yarlagadda, S., Advani, S., Deitzel, J., Heider, D., Molligan, D., Roseman, D., Simacek, P., Tierney, J., & Gillespie, J. W. (2019). Formability of TuFF Composite Blanks. In: SAMPE 2019 - Charlotte, NC. Proceedings
6. Henry Fidlow, Thomas A. Cender, Pavel Simacek, Shridhar Yarlagadda, Suresh G. Advani Extensional Viscosity of Thermoplastic TuFF Composites in Stretch Forming Processes In: SAMPE 2022 - Charlotte, NC. Proceedings
7. Creasy, T. S., & Advani, S. G. (1997). A model long-discontinuous-fiber filled thermoplastic melt in extensional flow. *Journal of Non-Newtonian Fluid Mechanics*, *73*(3), 261–278. https://doi.org/10.1016/S0377-0257(97)00045-1
8. Šimáček, P., & Advani, S. G. (2019). A micromechanics model to predict extensional viscosity of aligned long discontinuous fiber suspensions. *International Journal of Material Forming*, *12*(5), 777–791. https://doi.org/10.1007/s12289-018-1447-y
9. Slange, T. K. (2019). Rapid Manufacturing of Tailored Thermoplastic Composites by Automated Lay-up and Stamp Forming (University of Twente).

6. ACKNOWLEDGEMENTS

This material is based upon work supported by the National Aeronautics and Space Administration under Grant and Cooperative Agreement No. 80NSSC20M0164, issued through the Aeronautics Research Mission Directorate, Transformative Aeronautics Concepts Program, University Leadership Initiative.